Planet. Space Sci., Vol. 31, No. 10, pp. 1147–1155, 1983
Printed in Great Britain.

0032-0633/83 $3.00 + 0.00
Pergamon Press Ltd.

PITCH-ANGLE SCATTERING OF ENERGETIC PROTONS IN THE MAGNETOTAIL CURRENT SHEET AS THE DOMINANT SOURCE OF THEIR ISOTROPIC PRECIPITATION INTO THE NIGHTSIDE IONOSPHERE

V. A. SERGEEV, E. M. SAZHINA and N. A. TSYGANENKO
Institute of Physics, Leningrad State University, Leningrad 198904, U.S.S.R.

and

J. Å. LUNDBLAD and F. SØRAAS
Dept. of Physics, University of Bergen, N-5014 Bergen, Norway

(*Received* 20 *January* 1983)

Abstract—Characteristics of the nightside isotropic precipitation of energetic protons during a period of 4 quiet days has been studied using data from the ESRO 1A satellite. The observed features of the equatorward precipitation boundary (its thickness, energy dependence, dynamics, dependence of its latitudinal position on the magnetic field at the geosynchronous orbit, etc.) were found to be in good agreement with calculations based on recent magnetospheric magnetic field models. We argue that the mechanism of non-adiabatic pitch-angle scattering in the equatorial current sheet is a dominant source of isotropic precipitation of energetic protons observed in the nightside auroral zone. Observations of the isotropic precipitation boundary can be used for monitoring the changes in the magnetotail current intensity.

1. INTRODUCTION

The presence of a thin current sheet in the nightside part of the magnetosphere leads to many important processes which control the dynamics and distribution of the energetic particle population. One of its most essential consequences is a strong pitch-angle scattering of particles due to violation of the first adiabatic invariant $\mu = E_\perp/B$. Acceleration and scattering of particles in the current sheet has been studied by several authors, i.e. Speiser (1965) and Lyons and Speiser (1982). The details of this mechanism were studied by West *et al.* (1978) with application to probing the near-equatorial magnetic field configuration. In a recent paper by Tsyganenko (1982) a numerical investigation of the nonadiabatic scattering mechanism has been made with emphasis on the problem of equilibrium distribution functions. Sergeev and Tsyganenko (1982) have considered the consequences of this process for the overall distribution of particles in the outer radiation belt and their loss times. It has been shown, in particular, that the nonadiabatic particle scattering in the equatorial current sheet provides a rapid filling of the ionospheric loss cone, so that a significant part of the energetic particle precipitation into the ionosphere can be explained by this mechanism, which depends only on the magnetotail current intensity and its spatial distribution. Therefore, the observations of particle precipitation boundaries at low-altitude polar orbiting satellites can serve as a convenient tool for diagnostics of the magnetotail current magnitude and its temporal evolution. With this important application in mind, we shall proceed with further investigation of the problem.

The present study is devoted to a comparative analysis of some features of energetic proton precipitation observed by the low-orbiting satellite ESRO-1A during an extended quiet period and those obtained from calculations using a recent version of an empirical model of the magnetospheric magnetic field. The most important parameter for our purposes (and for future applications) is the latitude of the equatorward boundary of isotropic precipitation belt, Λ_i. We are primarily interested in investigating the characteristics of this boundary (its thickness, position, rigidity dependence, etc.), compared to the corresponding model results, and to study its dependence on the intensity of the magnetotail current. As an approximate measure of the latter we shall use the magnitude of the magnetic field at the Equator in the midnight portion of the geosynchronous orbit. This choice is reasonable for comparisons with energetic proton characteristics, because, as we shall show later, the innermost boundary of their non-adiabatic pitch-angle scattering is located in the midnight sector just in the vicinity of the geosynchronous distance. The results of our com-

parison show that all the essential features of the proton precipitation during the studied quiet period agree well with the discussed mechanism.

A special word should be said about why just the quiet-time precipitation of energetic protons has been preferred for our comparative study. First of all, the selection of extended very quiet periods most probably minimizes the influence of scattering due to particle interactions with electromagnetic waves which, in principle, also could be an effective source for the pitch-angle diffusion. Secondly, during quiet periods, the effects of impulsive injections and accelerations of fresh particles are also minimal and the trapped particles are distributed more or less uniformly around their drift-shells. This allows us to overcome some special difficulties arising due to details of the satellite orbit (see Section 3). The choice of energetic proton data for this study is based on the estimates for the particle loss times made by Sergeev and Tsyganenko (1982). They have found (and our data support this finding) that for stable magnetospheric conditions only proton precipitation can be observed during tens of hours. During quiet times the isotropic energetic electron precipitation zone would be located at higher latitudes, but the electron losses are very rapid in this region, so that the electron flux falls off on a time scale of the order of one period of revolution of the low-orbiting satellite. For a further discussion of the electrons see Section 6.

In the next section the results of our model calculations concerning the ionospheric loss cone filling are considered and we examine the features of particle precipitation based on recent magnetospheric magnetic field models. In Section 3 we shall describe the method used for determination of the quantity Λ_i from ESRO-1A data; Section 4 deals with the observed features of the isotropic precipitation zone. The last two Sections, 5 and 6, are devoted to a comparison between experimental and model results with a subsequent discussion of their application to the problem of the magnetotail current diagnostics.

2. MODEL CALCULATIONS

The main parameter which controls the degree of pitch-angle scattering of particles with small pitch angles (we use hereafter the pitch angles reduced to their equatorial values, θ_e, by using the adiabatic law) is $K = R_c/\rho$. Here $R_c = B_z/(\partial B_x/\partial z)$ is the field line curvature radius at the equator, $\rho = mV/eB_z$ is the Larmor parameter estimated from the total particle velocity, V. With the aim to define the spatial boundary of particles which are scattered isotropically over the ionospheric loss cone, we shall introduce some "critical" value K_{CR} corresponding to a rapid change in the degree of the loss cone filling. To relate the parameter K with the flux of particles precipitating into the loss cone, we have done a detailed calculation of the pitch angle distributions in the scattered particle beams.

A simple model magnetic field of the tail current sheet has been adopted, being identical to that used in the work by Tsyganenko (1982). We considered an initial beam of particles with small pitch angles incident upon the magnetic field reversal region. The corresponding pitch angle distribution in the incident beam was assumed to be isotropic outside the loss cone, with no particles in the loss cone as it is shown in Fig. 1 by broken lines, i.e. $J = 1$ for $\theta^i \leqslant \theta_e \leqslant \theta^B$ and $J = 0$ for $\theta_e < \theta^i$. Here J denotes the particle flux (in relative units) per unit solid angle, θ^i corresponds to the loss cone boundary and θ^B is the upper limit of the studied pitch angle interval. Each particle trajectory has been tracked until its emergence into the region of adiabatic motion with the uniform magnetic field on the other side of the current sheet (details of trajectory computations can be seen in the paper by Tsyganenko (1982)). The final pitch angle distributions in the scattered beam are shown in Fig. 1 by solid lines. Both initial and final pitch-angle distributions in Fig. 1 are normalized to equal solid angle intervals, i.e. they correspond to the measured unidirectional differential particle flux. The total number of particle trajectories tracked in each run (that is, for each set of model parameters) was 3000; this corresponds to 50 pitch angle values between θ^i and θ^B and 60 equidistant gyrophase values for each pitch-angle. The upper limit of the pitch angles was $\theta^B = 8.4°$, the absence of contribution of particles coming from outside this limit to the flux into the loss cone being controlled additionally.

The ionospheric loss cone width $\theta^i = 2.5°$, chosen in the case shown in Fig. 1, corresponds to the equatorial magnetic field value $B_z = 95$ nT, provided $B = 5 \cdot 10^4$ nT in the ionosphere. The magnetic field outside the current sheet is inclined to the equatorial plane by $\alpha = 45$ (i.e. $B_x = B_z$ outside the field reversal region) for the case of Fig. 1. These features are typical for conditions in the vicinity of the geosynchronous orbit in the nightside region; we note, however, that the results presented below do not reveal any significant dependence on the particular choice of reasonable values of both α and θ^i.

As can be seen from Fig. 1, the scattered particles appear at the centre of the loss cone for $K \lesssim 8$ and the loss cone is filled completely for $K \lesssim 6$ (the strong diffusion limit). Thus, for the particular case of our ESRO-1A proton measurements (narrow angle detectors directed strictly along and perpendicular to the field line) we adopt a condition $K_{CR} = 8$ as a

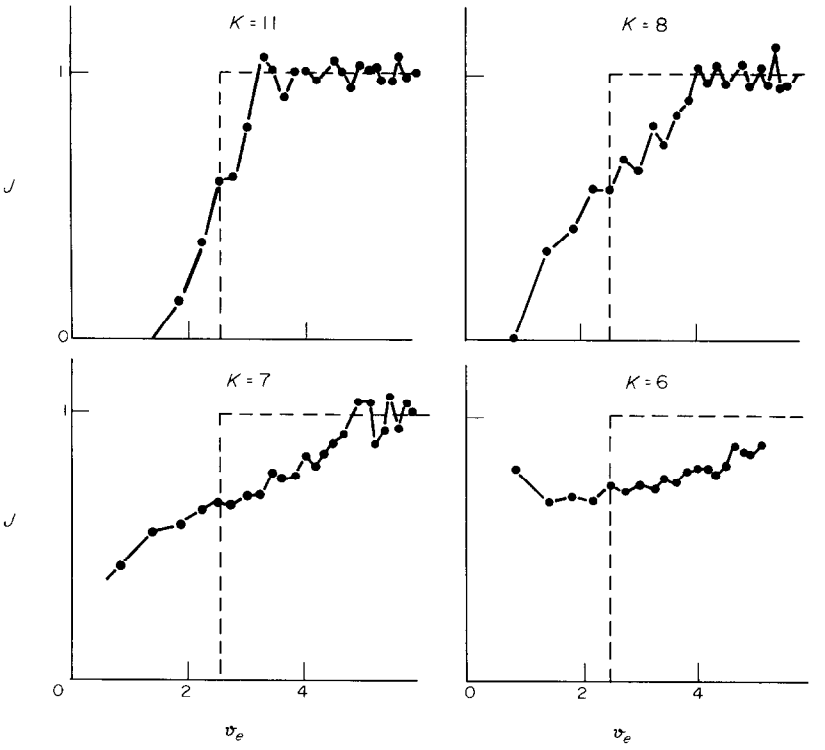

FIG. 1. ANGULAR DISTRIBUTION OF THE UNIDIRECTIONAL PARTICLE FLUX BEFORE (BROKEN LINES) AND AFTER (SOLID LINES) SCATTERING OF THE PARTICLE BEAM IN THE CURRENT SHEET REGION, FOR DIFFERENT VALUES OF THE PARAMETER $K = R_c/\rho$.
Initial distribution (before scattering) was assumed to be isotropic with an empty loss cone.

convenient definition of the innermost boundary of isotropic precipitation.

To calculate the position of this "isotropy boundary" (IB) in the magnetotail and to determine its projection into the ionosphere, we have used a new version of an empirical magnetospheric magnetic field model developed recently by Tsyganenko and Usmanov (1982). Compared with earlier models (Mead and Fairfield, 1975), it is based on a more extensive data set, providing more realistic representation of the main magnetic field sources and contains a more detailed dependence on the K_p-index. The last feature enables us to study the change in IB location caused by the growth of the magnetotail current intensity. The main results pertaining to the midnight meridional cross-section are shown in Fig. 2 and in Table 1. They will be used later, in a comparison with the experimental data; one important point, however, should be mentioned.

As is evident from Table 1, the IB for the 150-keV protons is located at the night side near geosynchronous orbit for a wide range of the disturbance level. This opens a possibility for direct comparison of both model and experimental values of Λ_i with the value of B at the

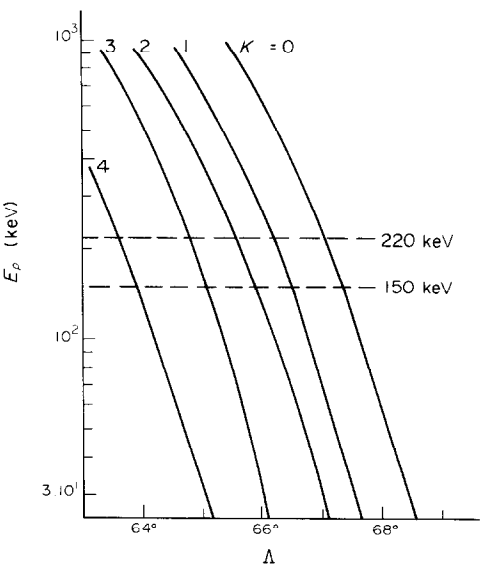

FIG. 2. POSITION OF THE ISOTROPIC PRECIPITATION BOUNDARY ($K = 8$) AT THE MIDNIGHT, Λ_i, VS PROTON ENERGY, CALCULATED FOR SEVERAL K_p VALUES USING THE MAGNETOSPHERIC FIELD MODEL OF TSYGANENKO AND USMANOV (1982).

TABLE 1. CALCULATED PARAMETERS FOR FIELD FLUX TUBES CROSSING AT GEOSYNCHRONOUS DISTANCE (6.6 *Re*) AND THE SAME PARAMETERS FOR FLUX TUBES CORRESPONDING TO THE POSITION OF THE ISOTROPIC BOUNDARY OF 150 keV PROTONS AT THE MIDNIGHT.

The values are given for a number of K_p values

	$X = -6.6\ Re$		Isotropic boundary ($K = 8$)		
K_p	B_z^e (nT)	$\Lambda_{6.6}$	x (Re)	B_z^e (nT)	Λ_i
0	89.0	65.9°	−7.8	49	67.3°
1	84 3	65.5°	−7.55	52	66.5°
2	81.9	65.1°	−7.4	55	65.9°
3,3+	75.9	64.7°	−7.0	61	65.1°
>4	73.9	63.9°	−6.65	72	63.9°

Equator (determined roughly from the H-component measured by ATS-1 satellite). By means of such a comparison we can check the consistency of the discussed mechanism with experimental data and link directly the observed boundary position, Λ_i, with the intensity of the magnetotail and ring currents.

3. DETERMINATION OF THE "ISOTROPY BOUNDARY" LATITUDE FROM THE ESRO-1A OBSERVATIONS

The data used in this paper are from the S71C experiment on board the magnetically stabilized polar orbiting satellite ESRO-1A. During the studied period the satellite orbit was approximately in the noon–midnight meridian plane passing over the southern and northern auroral zones. We use data from narrow angle detectors directed parallel and perpendicular to the local magnetic field. The instrument sampled protons in the ranges 115–180 (150–215) keV and 210–350 (225–360) keV; the values in parentheses pertain to the detectors oriented perpendicularly to the magnetic field. A detailed description of the instrument is given by Søraas *et al.* (1970). In the low-speed mode of operation a complete sample of measurements was obtained every 3.6 s which corresponds to approx. 0.2 latitude resolution over the auroral zone.

With reference to Fig. 1 it seems that the simplest way to derive the location Λ_i of the IB from the measured particle fluxes is to find the latitude interval, where the ratio of precipitating to trapped flux rises rapidly to unity. However, due to the geometry of the experiment and magnetic stabilization of the satellite, the parallel detectors measure the precipitating flux (in the centre of the loss cone) only in the Northern Hemisphere, which leads to some problems in derivation of Λ_i from ESRO-1A data. A typical example of particle fluxes at the night side during consecutive southern and northern traversals of the auroral zone is shown at the top of Fig. 3. As can be seen from this and all other examples studied, the locally trapped particle fluxes differ drastically in the Northern and Southern Hemispheres at latitudes below the region of intense isotropic precipitation. The reason for this discrepancy lies in the different satellite altitude in the opposite hemispheres, around 400 km in the northern and around 1500 in the southern. The particles which would mirror locally around 400–500 km are lost in the ionosphere, as they drift around the Earth. This occurs due to large variations of their mirror point heights caused by a large inhomogeneity of the Earth's magnetic field (Cole and Thomas, 1968; Berg and Søraas, 1972). Because of this, to avoid large errors in the derivation of Λ_i, we compare the precipitating flux, $J_{\parallel}$, from the northern pass to the trapped flux, $J_{\perp}$, from the consecutive

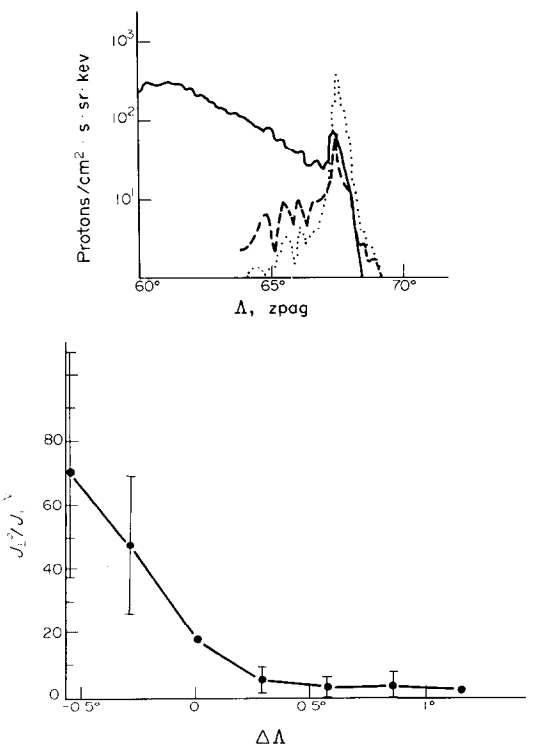

FIG. 3. (a)—PROFILES OF LOCALLY TRAPPED (150–215 keV, DENOTED AS $J_{\perp}$) AND PRECIPITATING (115–180 keV, DENOTED AS $J_{\parallel}$) PROTON FLUX MEASURED BY THE ESRO-1A SATELLITE DURING THE CONSECUTIVE SOUTHERN (16.20 U.T.) AND NORTHERN (16.58 U.T.) NIGHTSIDE TRAVERSALS OF THE AURORAL ZONE ON 22 OCTOBER 1968, VS INVARIANT LATITUDE. (b)—average $J_{\perp}^s/J_{\parallel}^N$ ratio profiles vs invariant latitude, obtained by a superposition of 14 individual profiles with a reference to the point $J_{\perp}/J_{\parallel} = 20\,(\Lambda_i)$. Vertical bars denote the S.D. of individual values.

southern pass. This could introduce a small error in the determination of Λ_i.

The most likely error could be caused by fast variations in the magnetospheric state during the 30 min between these traversals. In order to minimize this error we limit ourselves to consider only a very long quiet period. By comparing the southern profiles of trapped particles taken from consecutive orbits during this time period, we usually found only minor variations around the expected Λ_i value. The values were within the range of small-scale perturbations of the intensity profiles and hence, this source of errors seems to be insignificant. Also, we checked the absence of a marked local time variation of the trapped particle profiles during the period study. Such variations could introduce additional errors when comparing the Northern and Southern Hemisphere data from different (within 22–03 h of eccentric dipole time) local time sectors during a more active period.

As can be seen from Fig. 3, the precipitating flux, $J_{\parallel}^{N}$, falls off abruptly at the equatorial edge of the intense precipitation region, whereas the trapped flux, $J_{\perp}^{S}$, rises steadily and does not display any systematic changes in this region. Because of this feature a minor error in the $J_{\perp}^{S}$ values are not believed to affect significantly the derived value of Λ_i. For a more accurate determination of Λ_i we have chosen a somewhat arbitrary value of the ratio $J_{\perp}^{S}/J_{\parallel}^{N} = 20$, lying somewhere in the central part of the boundary region. A correction for the different energy windows of parallel and perpendicular detectors has been made by approximating the energy spectrum with the power law $E^{-\gamma}$, using the two different energy channels of the perpendicular detector. Usually this yielded a $\gamma = 5$–6 in the region of interest.

The profiles of the $J_{\perp}/J_{\parallel}$ ratio vs invariant latitude, Λ, were superimposed on each other with reference to the point Λ_i (with $J_{\perp}/J_{\parallel} = 20$) to find the average behaviour of $J_{\perp}/J_{\parallel}$ in the boundary region. The results for 14 passes are given in the bottom of Fig. 3. On the average, Λ_i is located 0.3–0.5° equatorward of the flat portion of the $J_{\perp}/J_{\parallel}$ profile which corresponds to the isotropic precipitation region. The $J_{\perp}/J_{\parallel}$ ratio changes by an order of magnitude across this transition region centered at Λ_i, within a 0.6° interval of invariant latitude.

4. FEATURES OF THE ISOTROPIC PRECIPITATION ZONE DURING A PROLONGED QUIET PERIOD

Geomagnetic activity indices and the energetic proton precipitation parameters for the nightside region are given in Fig. 4. The used 4-day period is the most prolonged interval of quietness during the whole time of ESRO-1A operation. The K_p and A_E activity indices were, respectively $\lesssim 1$ and $\lesssim 50$ nT during most of this period. Only a few brief southward excursions of the IMF and corresponding signatures of small substorms were observed. In spite of the absence of intense substorms, a steady proton precipitation was observed in each ESRO-1A pass during this time, covering 2–4° interval of latitude between Λ_i and Λ_b (background boundary) as shown in Fig. 4.

In Fig. 5 four latitudinal profiles of trapped particle fluxes are compared. Due to the 103-min orbital period, each fourteenth satellite orbit was located roughly at the same geographical longitude. The satellite orbit is fixed in local time. Thus, a direct comparison of the trapped particle intensity profiles can be used to evaluate the time scale of particles losses in the isotropic precipitation regime (strong diffusion limit), assuming no particle injection. By comparing the data in Fig. 5, which spans the 72-h interval between 04.00 U.T. on 21 October and 04.00 U.T. on 24 October, we do not find any reduction in the trapped 150-keV proton fluxes in the isotropic precipitation zone, that is in the 65–69° interval of latitude. Such low loss rate of energetic protons into the ionosphere is consistent with the calculations of Sergeev and Tsyganenko (1982). For 100-keV protons they estimated the loss time due to the isotropic precipitation to be several tens of hours. It follows also from their results, that much more rapid ($T \sim 1$ h) losses should occur at higher invariant latitudes, at field tubes with developed drift loss cone for the near-equatorial particles. The boundary of this region can be associated with the background boundary latitude, Λ_b, in the trapped proton fluxes.

The observed tendency of the precipitation zone shifting towards higher latitudes (Figs. 4 and 5) reveals an obvious correspondence to the increase in both the *Dst*-index and the H-component of the magnetic field at geosynchronous distance. Thus, such a shift results apparently from the DR- and/or tail current reduction and re-distribution. A study of this phenomenon constitutes a separate problem and demands an additional analysis. Several more short-lived transient latitudinal shifts of the IB are superimposed on this long-term trend. These variations are clearly associated with the changes of the maximum intensity of precipitating protons, $J_{\parallel}^{\max}$, so that this quantity increases when the IB shifts equatorwards (Fig. 4). Sometimes these shifts are associated with southward excursions of IMF and corresponding growth phase phenomena (see, for example, the intervals around 10.00 U.T. on 21 October, 18.00 U.T. on 23 October and 16.00 U.T. on 24 October). In other cases the signatures in A_E and IMF were not so clear. However, these variations can be associated with small substorms, with

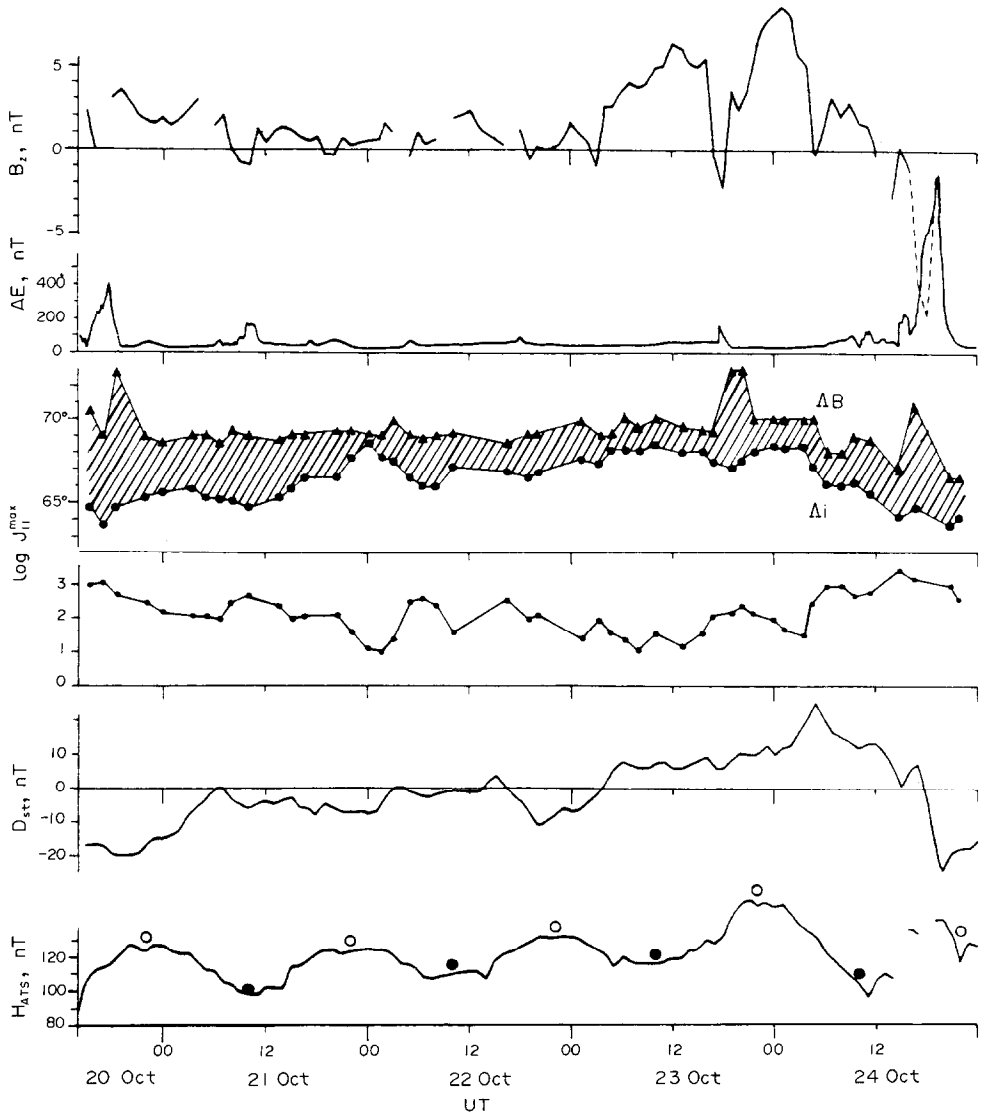

FIG. 4. SUMMARY OF ACTIVITY DURING THE PERIOD OF 20–24 OCTOBER 1968.
From the top to the bottom: IMF B_z—component (hourly average values from King, 1977); A_E-index, position of the proton precipitation boundaries at the nightside and the maximum fluxes of precipitating protons—both from ESRO-1A measurements; *Dst*-index; H-component of the magnetic field measured at the ATS-1 satellite. Solid and open circles in the bottom part denote, respectively, the local midnight and noon at the ATS-1 position.

corresponding variations of the tail current intensity; we shall discuss this point in more detail in Section 6.

5. COMPARISON OF MODEL AND EXPERIMENTAL DATA CONCERNING THE "ISOTROPY BOUNDARY"

The first quantity that should be discussed in this respect is the thickness of the IB. According to our model calculations (see Fig. 1), a replacement of $K = 8$ (which corresponds just to a first appearance of scattered particles in the centre of the loss cone) by $K = 6$ (almost complete filling of the loss cone) results in a 0.4–0.5° shift of the ionospheric projection of the corresponding boundary. This estimate appears to be the same for each of the K_p levels of our magnetospheric models and agrees well with the experimentally

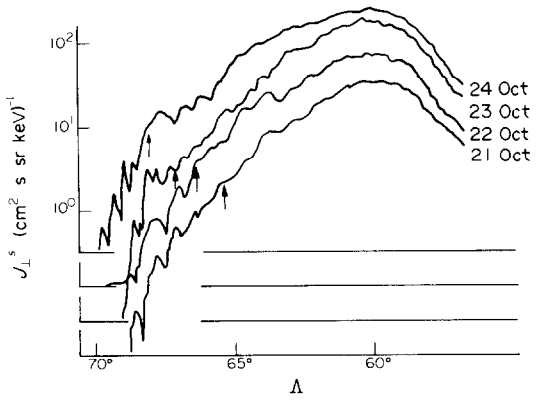

FIG. 5. FOUR LATITUDINAL PROFILES OF TRAPPED 150-keV PROTON FLUX, OBTAINED DURING A PROLONGED QUIET PERIOD. The profiles were obtained approximately once a day. Together, they span 72 h of the quiet-time period. The IB positions are indicated by arrows.

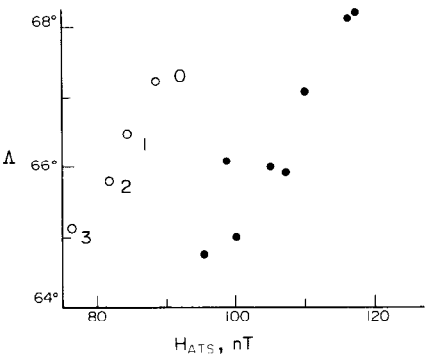

FIG. 6. SOLID CIRCLES—COMPARISON OF SIMULTANEOUS VALUES OF Λ_i, DEDUCED FROM ESRO-1A LOW-ALTITUDE MEASUREMENTS, WITH THE H-COMPONENT OF MAGNETIC FIELD AT THE GEOSTATIONARY ORBIT OF ATS-1, WHEN BOTH SATELLITES WERE LOCATED AT THE NIGHTSIDE WITHIN 2 h M.L.T. FROM ONE ANOTHER.
Open circles denote the results of model calculations, taken from Table 1. The large discrepancy between model and experimental values is mainly due to uncertainty in the reference level of the ATS-1 data.

measured width of the latitude interval within which the ratio $J_\perp/J_\parallel$ changes by an order of magnitude (see Section 4 and Fig. 3).

The next comparison concerns the energy dependence of the IB position. We have determined Λ_i (from the condition $J_\perp/J_\parallel = 20$) at two energy ranges (>150 and >220 keV) for 24 quiet-time passes of ESRO-1A. The average latitudinal difference for these cases appeared to be $\Delta\Lambda = \Lambda_i$ (150 keV)$-\Lambda_i$ (220 keV) $= +0.6°$, with a 0.5° S.D. The corresponding value derived from our model calculations (see Fig. 2) is $\Delta\Lambda = +0.4°$. In view of limitations imposed by ESRO-1A spatial resolution ($\sim 0.2°$), the presence of noise and possible small errors arising from comparing the northern ($J_\parallel$) and southern ($J_\perp$) data, these two values seem to be in a good agreement.

The third comparison is of special importance and concerns the relation of the IB position to the tail current intensity. Here we have used the magnetic field data from the geostationary satellite ATS-1 (Coleman and McPherron, 1976), situated at 150° W longitude, that is near the line of intersection of the geomagnetic and the geographic equatorial planes. The comparison has been carried out only for the 08.00–10.00 U.T. intervals of the 4-day period, so that the ATS-1 position falls within the 22.00–24.00 M.L.T. sector and thus corresponds approximately (within 1–2 h) to the M.L.T. sector of the ESRO-1A nightside pass. The results of the comparison are given in Fig. 6 (solid circles) along with the corresponding calculated data taken from our Table 1. As can be seen in the figure, a well-pronounced correlation does exist between changes in Λ_i and H_{ATS} as well as a marked difference between the experimental and model points. To explain this discrepancy, we note that the ATS-1 experimenters had problems with spacecraft-induced magnetic fields which eventually led them to a somewhat arbitrary choice of the H-component reference level. Later, Coleman and McPherron (1976) have found that the ATS-1 H-component values should be reduced by ~ 15–20 nT. Because of the uncertainty of this correction value we do not incorporate it in our results shown in Fig. 6; however, it is clear from the figure that just a -20 nT correction of the observed values of H_{ATS} removes the discrepancy between model and experimental points. This feature lends additional support to our conviction that a good agreement exists between model predictions and experimental data. The dependence of the IB latitude on the equatorial magnetic field magnitude at 6.6 *Re* is significant: Λ_i decreases by approx. 1.5° per 10 nT reduction in H_{ATS}.

6. DISCUSSION AND CONCLUSION

The discussed mechanism for the strong pitch-angle scattering of energetic particles in the magnetospheric equatorial current sheet (DR plus tail current) leads to a nearly isotropic precipitation of particles in the magnetic field line tubes, where the following condition is met

$$K = B_z^2(\partial B_x/\partial z)^{-1}(mV/q)^{-1} \lesssim K_{CR}$$

where $K_{CR} \approx 8$ and K depends only on the particle mass, energy and charge and on the magnetic field distribution in the equatorial magnetosphere. Thus, we

should observe precipitating particles over the nightside ionosphere, being isotropic over the loss cone, in any magnetic flux tube outside the field line surface having $K = K_{CR}$ (i.e. with $\Lambda > \Lambda_i$), provided there exists a sufficient amount of previously injected trapped radiation. This prediction is well confirmed by the measured characteristics of the proton flux in any satellite pass over the nightside auroral zone, irrespective of the intensity or phase of magnetospheric disturbance (see Figs. 3 and 4, and also the work by Lundblad *et al.*, 1979). Sometimes, during the so-called "leap" phase at the end of a substorm (Lundblad *et al.*, 1979) this isotropic precipitation zone extends in latitude over more than 5–10° and is observed up to $\Lambda \gtrsim 75$. We know of no other single mechanism that can operate steadily in the "strong diffusion" regime in the vast region from geostationary orbit up to the far magnetotail, because of drastic changes in the physical conditions (particle flux, plasma density and pressure anisotropy, magnetic field, Alfvén velocity, etc.) observed over this large range of distances.

In our mind, this single mechanism can easily explain the usually observed dependence of Λ_i on particle rigidity, displayed in any magnetospheric conditions (see also Søraas *et al.*, 1977; West *et al.*, 1978; Imhof *et al.*, 1979). These considerations, along with the good consistency of predicted and experimental properties of the IB, demonstrated in the previous section, indicates the important role of this mechanism in maintaining the isotropic precipitation, at least for energetic protons and heavier particles.

Some other experimental facts are well accounted for by this mechanism. One of them is the absence of isotropic precipitation under quiet conditions over the dayside ionosphere below the cusp latitude (Lundblad *et al.*, 1979), which are in accordance with model predictions. The next fact is the equatorward displacement of the IB with the associated growth of precipitating fluxes during periods of geomagnetic enhanced activity (Sørass *et al.*, 1977; Imhof *et al.*, 1979; Lundblad *et al.*, 1979; see also Fig. 4). In the framework of our model, this is explained simply by a decrease of the magnetic field in the equatorial inner magnetosphere caused by an increase of the tail currents (Russell and McPherron, 1973). Because of a strong dependence of K on B_z ($K \sim B_z^2$) the field line surface having $K = K_{CR}$ exhibits a marked earthward shift with the associated equatorward displacement of the IB over the ionosphere. The close correlation between Λ_i and H_{ATS} shown in Fig. 6 is a manifestation of this process. Also since the intensity of the previously trapped particle flux is larger at lower latitudes in the region of interest (see Figs. 3 and 5), the earthward displacement of the scattering boundary is accompanied by an enhancement of the maximal precipitating flux intensity as was found in Section 4.

So far we have focused our attention mainly on the energetic protons. Some words should be said also about the electrons. Although the discussed scattering mechanism operates also in case of electrons, several important differencies arise, because of lower rigidities and higher velocities of electrons, as compared to protons of the same energy. Due to the lower rigidity of electrons, their IB is situated at much larger distances in the tail, usually within the region of wide drift loss cone at the night side (Sergeev and Tsyganenko, 1982). This rigidity dependence was observed experimentally by West *et al.* (1978) and by Imhof *et al.* (1979). The second and more important difference (higher velocities) leads to much more rapid loss of the energetic electron population in the magnetic flux tubes, with a typical loss time of the order of 1 h (Sergeev and Tsyganenko, 1982). Therefore, in a steady or slowly varying magnetic field configuration the energetic electron content is relatively small in those magnetic flux tubes where the electrons are scattered isotropically over the loss cone. This feature is also in line with observations (Rossberg, 1978). During more active periods, when the rapid increase of the tail current shift the IB earthward on a short time scale, the difference between the electron and ion precipitation zones are less significant. For instance, during substorm growth phase a belt of steady energetic electron precipitation is observed, being narrow (1–2°) in latitude and extended in a wide longitudinal sector around the midnight (see Pytte and West, 1978, and references therein) and the electron precipitation increases and becomes more structured during substorm main phase. The latitudinal profiles of trapped and precipitating electrons in these events (Rossberg, 1976) are similar to that shown in Fig. 3a.

The results presented in this paper seem to open a new possibility for diagnostics of the magnetotail current intensity and for studying of the ring/tail current evolution at different stages of a magnetospheric disturbance by observing the particle precipitation, boundaries. Before this can be done, however, a detailed analysis of the IB on the magnetospheric disturbance level has to be performed. The present study indicates that there is a clear relation between the Λ_i value near midnight and the magnetic field magnitude at geosynchronous position: Λ_i changes by 1.5° per 10 nT of change in field magnitude. The protons have a sufficiently long lifetime to be precipitating isotropically also during prolonged quiet period. The advantage of such a method is a longterm continuous monitoring of the current sheet in real time (twice per satellite revolution)—this can be realized by using the energetic particle measurements on polar

orbiting satellites, covering a wide range of rigidities, together with realistic magnetospheric magnetic field models.

To summarize our main conclusions: (1) Pitch-angle scattering of energetic protons in the equatorial current sheet of the magnetotail is an important source of their continuously intense precipitation observed over the nightside auroral zone, during both active and quiet periods. This might even be the dominant mechanism by which high energy ions are precipitated, over a wide range of geomagnetic activity. (2) Observations of this isotropic precipitation zone can be used for monitoring changes in the magnetotail current magnitude.

Acknowledgements—The magnetic field data from the ATS-1 satellite, used in this study, were kindly provided by Dr J. Vette, National Space Science Data Center, through WDC-A (Rockets and Satellites). The ESRO I satellite program was conducted by the European Space Research Organization. This research was supported financially by the Royal Norwegian Council for Scientific and Industrial Research.

REFERENCES

Berg, L. E. and Søraas, F. (1972) Observations suggesting weak pitch angle diffusion of protons. *J. geophys. Res.* **77**, 6708.

Cole, K. D. and Thomas, F. A. (1968) Maps of difference in geomagnetic field at conjugate areas. *Planet. Space Sci.* **16**, 1357.

Coleman, P. J. and McPherron, R. L. (1976) Substorm observations of magnetic perturbations and ULF waves at synchronous orbit by ATS-1 and ATS-6, in *The Scientific Satellite Program during the International Magnetospheric Study* (Edited by Knott, K. and Batytrick, B.), pp. 345–365. D. Reidel, Dordrecht.

Imhof, J. W. L., Reagan, J. B. and Gaines, E. E. (1979) Studies of the sharply defined L dependent energy threshold for isotropy at the midnight trapping boundary. *J. geophys. Res.* **84**, 6371.

King, J. H. (1977) Interplanetary medium data book, Appendix, NSSDC report 77-04a.

Lundblad, J. Å., Søraas, F. and Aarsnes, K. (1979) Substorm morphology of >100 keV protons. *Planet. Space Sci.* **27**, 841.

Lyons, L. R. and Speiser, T. W. (1982) Evidence for current sheet acceleration in the geomagnetic tail. *J. geophys. Res.* **87**, 2276.

Mead, J. D. and Fairfield, D. H. (1975) A quantitative magnetospheric model derived from spacecraft magnetometer data. *J. geophys. Res.* **80**, 523.

Pytte, T. and West, H. T. (1978) Ground-satellite correlations during presubstorm magnetic field configuration changes and plasma sheet thinning in the near-Earth magnetotail. *J. geophys. Res.* **83**, 3791.

Rossberg, L. (1976) Prebay electron precipitation as seen by balloons and satellites. *J. geophys. Res.* **81**, 3437.

Rossberg, L. (1978) Undisturbed trapping boundary for energetic electrons. *J. geophys. Res.* **83**, 4307.

Russell, C. T. and McPherron, J. R. L. (1973) The magnetotail and substorms. *Space Sci. Rev.* **15**, 205.

Sergeev, V. A. and Tsyganenko, N. A. (1982) Energetic particle losses and trapping boundaries as deduced from calculations with a realistic magnetic field model. *Planet. Space Sci.* **30**, 999.

Speiser, T. W. (1965) Particle trajectories in model current sheets, 1. Analytical solutions. *J. geophys. Res.* **70**, 4219.

Søraas, F., Aarsnes, K., Lindalen, H. R. and Møhl Madsen, M. (1970) A satellite instrument for measuring protons in the energy range 0.1 MeV to 6 MeV. *Arb. univ. Bergen, Mat.–Naturv. serie no.* 6.

Søraas F., Lundblad, J. Å. and Hultqvist, B. (1977) On the energy dependence of the ring current proton precipitation. *Planet. Space Sci.* **25**, 757.

Tsyganenko, N. A. (1982) Pitch-angle scattering of energetic particles in the current sheet of the magnetospheric tail and stationary distribution functions. *Planet. Space Sci.* **30**, 433.

Tsyganenko, N. A. and Usmanov, A. V. (1982) Determination of the Magnetospheric current system parameters and development of experimental geomagnetic field models based on data from IMP and HEOS satellites. *Planet Space Sci.* **30**, 985.

West, H. I., Buck, R. M. and Kivelson, M. G. (1978) On the configuration of the magnetotail near midnight during quiet and weakly disturbed periods: magnetic field modelling. *J. geophys. Res.*, **83**, 3819.